Fuel Cell Modeling and Simulations

John Mantzaras[a*], Stefan A. Freunberger[a], Felix N. Büchi[a], Markus Roos[b], Wilhelm Brandstätter[c], Michel Prestat[d], Ludwig J. Gauckler[d], Bernhard Andreaus[a,e], Fia Hajbolouri[a], Stephan M. Senn[f], Dimos Poulikakos[f], Andreas K. Chaniotis[f], Diego Larrain[g], Nordahl Autissier[g], and François Maréchal[g]

---

[*]*Corresponence:* Dr. J. Mantzaras[a]

Tel:: +41-56-310 4046

Fax.: +41-56-310 2199

E-mail: ioannis.mantzaras@psi.ch

[a]Department of General Energy, Paul Scherrer Institute, CH-5232, Villigen PSI

[b]Center for Computational Physics, Zurich University of Applied Sciences Winterthur, Wildbachstrasse 21, Postfach 805, CH-8400 Winterthur

[c]Christian-Doppler-Laboratorium für Rechnergestützte Angewandte Thermofluiddynamik an der Montanuniversität Leoben, Franz-Josef-Strasse 18, A-8700 Leoben, Austria

[d]Nonmetallic Inorganic Materials, Department of Materials, Swiss Federal Institute of Technology, ETH-Zentrum, Sonneggstrasse 5, CH-8092 Zürich

[e]Presently at: Department of Chemistry, Simon Fraser University, 8888 University Drive, Burnaby, BC, Canada, V5A 1S6

[f]Laboratory of Thermodynamics in Emerging Technologies (LTNT), Institute of Energy Technology, Swiss Federal Institute of Technology, ETH-Zentrum, Sonneggstrasse 3, CH-8092 Zürich

[g]Laboratory of Industrial Energy Systems (LENI), Institute of Energy Sciences (ISE), Swiss Federal Institute of Technology (EPFL), CH-1015 Lausanne

Abstract

Fundamental and phenomenological models for cells, stacks, and complete systems of PEFC and SOFC are reviewed and their predictive power is assessed by comparing model simulations against experiments. Computationally efficient models suited for engineering design include the (1+1) dimensionality approach, which decouples the membrane in-plane and through-plane processes, and the volume-averaged-method (VAM) that considers only the lumped effect of pre-selected system components. The former model was shown to capture the measured lateral current density inhomogeneities in a PEFC and the latter was used for the optimization of commercial SOFC systems. State Space Modeling (SSM) was used to identify the main reaction pathways in SOFC and, in conjunction with the implementation of geometrically well-defined electrodes, has opened a new direction for the understanding of electrochemical reactions. Furthermore, SSM has advanced the understanding of the CO-poisoning-induced anode impedance in PEFC. Detailed numerical models such as the Lattice Boltzmann (LB) method for transport in porous media and the full 3-D Computational Fluid Dynamics (CFD) Navier-Stokes simulations are addressed. These models contain all components of the relevant physics and they can improve the understanding of the related phenomena, a necessary condition for the development of both appropriate simplified models as well as reliable technologies. Within the LB framework, a technique for the characterization and computer-reconstruction of the porous electrode structure was developed using advanced pattern recognition algorithms. In CFD modeling, 3-D simulations were used to investigate SOFC with internal methane steam reforming and have exemplified the significance of porous and novel fractal channel distributors for the fuel and oxidant delivery, as well as for the cooling of PEFC. As importantly, the novel concept has been put forth of functionally designed, fractal-shaped fuel cells, showing promise of significant performance improvements over the conventional rectangular shaped units. Thermo-economic modeling for the optimization of PEFC is finally addressed.

Keywords: multidimensional simulations of fuel cells; porous electrode structure characterization; state-space modeling of electrochemical reactions; thermo-economic optimization

1. Introduction

The modeling and simulation activities span the entire fuel cell (FC) research domain, namely single cells, stacks, and complete systems of both Polymer Electrolyte Fuel Cells (PEFC) and Solid Oxide Fuel Cells (SOFC). The models themselves, either phenomenological or more fundamental, have been implemented in a variety of numerical simulation tools and the resulting predictions have been further compared against a broad series of measurements. Experiments provide valuable insights into the underlying FC processes, as also discussed in the previous contribution on Diagnostic Methods. However, the measurements are rather tedious and their limited spatial resolution hinders the in-depth analysis of the interacting phenomena. Multidimensional models have thus become increasingly important for the description of the Membrane Electrode Assembly (MEA) electrochemical processes and for addressing key FC design issues. The flow field and the structure of the bipolar plate, for example, have a profound impact on the cell or stack performance and their full description necessitates a three-dimensional model. 3-D Computational Fluid Dynamics (CFD) models extended and adapted for FC have advanced during the last years [1], and are able to provide detailed simulations for a single fuel cell unit. For large stacks, the computational time required for extensive parametric studies is still prohibitive. For the latter case, the complexity can be reduced substantially by considering the prevailing exchange processes in the cell [2-4], while still retaining a model dimensionality higher than one. The present review contains both lower-dimensionality approaches, with emphasis on the physical aptness of the therein-incorporated models, as well as advanced models of fuel cell units.

Global models describing a single PEFC consider the dominant processes across the membrane (through-plane), which include the transport of water, protons, reactant gases and heat. The exchange processes parallel to the membrane (in-plane) are controlled mainly by the reactant gaseous flow along the supply channels. The coupling between both in- and through-plane processes can be achieved with a (1+1) dimensionality model, which has been shown [2] to reproduce the along-the-channel current distribution inhomogeneities. Another global modeling approach for cells, stacks, and entire systems is the volume averaging approach [5]. Therein, the effective transport and interaction parameters are calculated for each component with the help of computationally efficient

3-D models of the actual structures. The effective parameters are subsequently deployed in less complex models (mostly 2-D), which allow the simulation of full stacks or systems at a much-reduced computational cost. With this tool, many mechanisms in the HEXIS SOFC were investigated and optimizations were undertaken [6]. A combination of 2-D CFD modeling with averaged volume energy equations has been also used for the optimization of the HTceramix SOFC design [7]. The development of models with reduced geometric complexity has enabled the extension of the simulations to true engineering environments. The approach is currently extended to PEFC with the aim to improve the water management system at a stack level [2].

In addition to the previous global models, understanding the electrochemical reactions at the molecular level and identifying the rate-determining steps (*rds*) is a key task in the development of new materials and designs and in the optimization of the electrode performance. The electrochemical processes are highly complex and involve multiple *rds*, consecutive and parallel pathways as well as mass transport. One widespread and popular experimental technique to investigate fuel cell reactions is electrochemical impedance spectroscopy [8]. Therein, equivalent circuits of resistive, capacitive and inductive elements are directly fitted to the experimental impedance spectra. However, this approach is limited by its lack of physical insight and the ambiguous interpretation of the equivalent circuits in terms of reaction steps. The identification of electrochemical processes requires a more fundamental modeling approach. State-Space Modeling (SSM) [9,10] allows for numerical simulation of the electrochemical reactions. Meaningful relations between reaction models, electrochemical behavior and experimental parameters of interest –such as electrode potential and oxygen partial pressure– can be established and further compared with measurements. SSM has been used to study the electrochemical behavior of various reaction models for SOFC-relevant interfaces as well as for different types of electrodes [9-11]. More recently [12], SSM has been extended to PEFC in order to investigate the CO poisoning kinetics.

In simulating the MEA processes, CFD methods for the solution of the transport equations at the pore level become very expensive due to the required high spatial resolution. An efficient alternative analysis, particularly suited for mesoscopic flow

domains, is the Lattice Boltzmann (LB) Method [13]. In modeling fuel cells, two-phase flow phenomena and electrochemical reactions have to be considered. This is achieved by the implementation of a so-called continuum surface (CSF) model where interfacial surface phenomena are no longer applied as discrete boundary conditions but rather as smoothly-varying volume forces acting in the transition region between the phases [14]. A LB model under development [15] considers a statistical approach to characterize the structure of porous electrodes and it is based on low-order correlation functions that can be derived from microscopic imaging methods such as computer tomography (CT). Recent comparisons of the measured pressure drop in a real porous structure showed excellent agreement with simulations that employed an artificially generated geometry and the corresponding LB-based flow predictions.

The flow distribution and the related electrochemical transport in cells have been addressed recently with 3-D CFD and detailed transport models. This is becoming a trend because such models contain all the physics involved and can improve the understanding of the related phenomena in a non ad-hoc manner, a necessary condition for the successful development of the fuel cell technology. Such models need to be supported by side experiments providing both some needed constants and validation data. 3-D modeling was recently used to optimize SOFC operating with internal methane steam reforming [16]. Additional simulations have exemplified the significance of porous and novel fractal channel distributors for the fuel and oxidant delivery, as well as for the cooling of PEFC [17,18,47-49]. With reference to the fractal fuel cell concept [47,48], a functionality-optimized (constructal) double staircase FC design was recently demonstrated, showing excellent promise compared to traditional alternatives. In SOFC, the design of reformers (utilizing porous micro- and nano-structures and well as fractal micro channel designs) to produce hydrogen and the thermal integration of such reformers into a micro-SOFC unit is currently under investigation [50]. Finally, multi-objective approaches based on evolutionary algorithms were used for thermo-economic optimization of PEFC [19].

Discussion

Global models are presented first, with emphasis on their capacity to reproduce measured performance characteristics of large cells such as current density distribution. The description of SSM follows, presenting advances in the understanding of both PEFC and SOFC electrochemical kinetics. The LB model is then introduced and the methodology for characterization and reconstruction (for simulation purposes) of porous electrode materials is elaborated. A general 3-D modeling approach is outlined, with applications in the design of an optimized PEFC flow distributor and in simulations of a SOFC with internal steam reforming. Finally, thermo-economic optimization models for PEFC are presented.

2.1 (1+1) dimensional model for the description of lateral effects in large PEFC

One of the main challenges in the engineering of large-scale, high-performance and stable fuel cells is the attainment of a current density distribution as homogeneous as possible. In conjunction with the properties of the employed electrochemical components, the structure of the bipolar plate has an important influence on the performance of the cell or the stack. The gas flow design, in particular, influences the current distribution due to its direct impact on gas and water transport. Technical cells are usually cooled via a liquid coolant flow inside the bipolar plate. The limited coolant flow leads to lateral temperature gradients, which may also critically affect the water management and hence the current distribution. A reduced approach is presented next, considering only the predominant exchange processes in the cell [2-4], which allows for the investigation of lateral inhomogeneities at an affordable computational cost. The transport of water, protons, reactant gases and heat perpendicular to the membrane are linked to the exchange processes parallel to the membrane, which are dominated by the mass flow in the gas channels.

2.1.1 Model Considerations

A single PEFC with conventional gas distributors is considered. The goal is to assess the influence of operating conditions such as feed gas humidities, stoichiometric ratios and temperature on the along-the-channel current density distribution, and to identify the distinct underlying voltage loss mechanisms. In technical size cells with active areas of

several 100 cm^2, the model domain has an aspect ratio of about 10^3, i.e. tens of centimeters along the channel flow and several 100 μm across the flow. This suggests that transport phenomena in the along-the-channel direction, which influence the overall distribution of any arbitrary physical property ϕ ,are mainly governed by convection. The general steady-state transport equation becomes:

$$?(\rho\, u\phi) - \quad ?(\tilde{A} \quad \phi) = S\,, \qquad (1)$$

with ρ, u, Γ and S representing the density, convective velocity vector, transport coefficient and source term, respectively. The convection-to-diffusion ratio leads to the dimensionless Péclet number, $Pe = uL/\Gamma$, where L is a characteristic axial length. Formal application of Eq. (1) leads to $Pe \sim 10^{10}$ for technical cells characterized with long channels and high convective velocities. This indicates that convective transport inside the channel by far dominates parallel diffusive fluxes in the gas diffusion media or in the membrane. Transport in the spanwise direction may appear in meander-like flows at the border of distinct bundles of channels. This will, however, affect only the channels in direct proximity to the border and may be neglected to a good approximation for multicolumn meanders. Thus, in-plane transport perpendicular to the flow can be neglected and local transport through the MEA can be considered one-dimensional. Boundary conditions governing the local transports vary along the flow direction with the channel composition. The local reactant consumption and water balance, in turn, serve as source terms for the flow in the gas distributor. The resulting (1+1)-dimensional model is represented by slices through the cell coupled by the channel flow only; fluxes in the along-the-channel direction between adjacent slices within the MEA are assumed negligible, as explained above. The following transport phenomena were considered: (i) multi-component diffusion of gaseous species through the porous anode and cathode gas diffusion layers, (ii) flow of water both in liquid and gaseous phase through anode, cathode, and inside the channels, (iii) transport of electrons through the carbon electrodes, (iv) migration of protons through the electrolyte, (v) transport of water through the membrane by diffusion and electro-osmotic drag, (vi) electrochemical reaction at the catalyst layer, (vii) transport of reactants and two-phase transport of water in the channels, (viii) heat generation due to reaction and resistance, and its removal by the cooling water. The resulting model was applied for both co- and

counter-flowing fuel and oxidant streams. Current density distributions can be further calculated for cells consisting either of a single or a combination of these two flow regimes.

2.1.2 Application to PEFC

The developed model [2] was applied to a technical cell with the flow-field arrangement of Fig. 1 and further validated with locally resolved current measurements (see also contribution on Diagnostic Methods). The predicted current density distribution in a 200 cm^2 active area cell operated at 343 K with fully humidified air and dry hydrogen at a stoichiometry of two (for each flow) is also shown in Fig. 1. Comparisons between predicted and measured current densities in the four depicted segments of Fig. 1 are provided in Fig. 2 as a function of air stoichiometry for fully humidified gases. Herein, the starvation of oxygen along the air path is evident.

Temperature inhomogeneities, which are driven by the specific type of cooling, can be a viable tool for FC performance optimization. For example, the effect of temperature increase along the coolant flow due to decreasing cooling water flow is illustrated in Fig. 3. Therein, the coolant flow is parallel to the co-flowing gases (from left to right in Fig. 3) and the cell is operated with dry air and wet hydrogen. As soon as the temperature towards the outlet reaches a value where the entire water product remains in the gas phase, the membrane water content decreases; this leads to a drop in the local current density that, in turn, gives rise to a more homogeneous current density distribution.

2.2 Volume averaging modeling in PEFC and SOFC

2.1.1 Model Considerations

The volume averaging models are characterized by their hierarchical structure. Cell and stack models contain fewer geometrical details and rely on phenomenological interaction terms, which are provided by lower-level numerical submodels. For example, mass transport in complex flow fields is described in an averaged manner with the help of effective material parameters. To establish the approach on basic principles, more detailed 3-D models derived from the true geometric structures are used to numerically evaluate the effective parameters [5]. This is reminiscent of the so-called Volume-Averaging-Method

(VAM) [20], which was developed to deduce effective transport equations with purely analytical means. In the model implementation, numerical simulations are used to perform the averaging, i.e. the effective parameters are obtained numerically, justifying the term Numerical-VAM (NVAM). While some rigor is lost compared to the analytical parent method, a lot of flexibility is gained, which is very important regarding the complexity of FC interactions. The simulation models at the top level no longer address details on the length scales below; however, they are modest with respect to CPU resources and are suited for parametric studies and investigation of full systems. In any case, the effective material and system parameters are based on the true geometry, which is used to study the influence of structural changes. The method can be validated intrinsically by testing the averaging process with the help of detailed models built form first principles.

2.2.2 Application to PEFC

Figure 4 illustrates a typical PEFC structure: meander flow fields transport hydrogen and air, respectively, to the MEA reaction zones. While it is possible to describe transport phenomena locally by the NVAM, there is no preferential direction to reduce the number of spatial dimensions. However, due to the fact that the flow is predominantly in-plane, it is still possible to work with planar models: two separate 2-D domains are used to describe the transport of the gaseous species in the anode and cathode as shown in Fig. 4 (bottom). These domains are coupled to each other by the electrochemical interaction, approximated by suitable interaction terms, as also described in the (1+1) model of Section 2.1. The geometric structure of the bipolar plates is cast into a spatially variable and strongly anisotropic permeability tensor. Unlike a true 3-D model, the electrochemical half-reactions are no longer described as heterogeneous surface interactions but are cast into "pseudo-volume" reactions, expressed as source terms within the 2-D domains. The rates are given in terms of the local physical quantities, i.e. molar fractions, pressure, and temperature. They have to be chosen carefully to approximate the net effect of the electrochemical processes. For realistic description of the MEA, these expressions cannot be expressed by analytic formulas due to the inherent complexity of transport processes in Nafion membranes. Therefore, one resorts to the numerical simulation of the relevant phenomena in 1-D (see Weber and Newman [21] and references therein).

The 2-D transport equations are discretized with the finite element method (FEM) and simulated within NM SESES, a general purpose CAE tool [22]. The 1-D numerical treatment of the electrochemical interactions relies on the shooting method for systems of coupled ordinary differential equations. The non-local coupling of the two separate 2-D domains represents the main issue with respect to a successful implementation. In standard FEM, strictly local interactions are usually addressed. In fact, NM SESES allows for the specification of source terms depending on non-local degrees of freedom (DOF). This provides the correct solution, but affects the convergence properties. With the help of decompositions of the DOFs into suitable subsets, which are solved iteratively in Gauss-Seidel loops, the obtained convergence performance is satisfactory. The discretization of 2-D domains for technically-relevant flows leads to a few thousand non-locally coupled finite elements. The 1-D transport model has to be solved at every FEM integration point and iteration. Overall, this approach is very promising. The number of DOFs for typical models and the necessary computer resources are at least an order of magnitude smaller than those of comparable 3-D models. As an illustration, Fig. 5 provides the molar fraction of water in the cathode and the anode compartment of a PEFC. The internal states within the MEA are also accessible: the species concentrations and the electrical potential near the hydrogen inlet are illustrated in Fig. 6.

2.2.3 Application to SOFC

The Sulzer HEXIS fuel cell stack [23] allows for an averaged description, exploiting the nearly rotational symmetric geometry. In an automated procedure, the effective parameters for the axisymmetric model are evaluated by using smaller 3-D flow-field models providing heat and electric conductivities as well as the permeability. These quantities are expressed by tensors, because the transport within the averaged structure becomes anisotropic. Similarly, averaged kinetic parameters for the electrochemical and the chemical interactions are also obtained. So far, these numerical models were successfully used to investigate SOFC performance including the radial temperature distribution and allowed for the optimization of cell and stack dimensions [6,24].

In another approach, the gPROMs package (general Process Modeling system [25]) is used to develop a fast sensitivity and optimization analysis tool. The repeat element

model (HTceramix SOFC stack design) combines a 2-D fluid flow description with averaged volume energy equations [7]. Flow field, fluid and solid temperature field and rates of reaction are computed. Parameters for the electrochemical model are introduced from experimental values obtained on small test cells of the same materials. To validate the model, experimental data (current-voltage) measured on full repeat elements (50 cm^2 cells including gas distribution and metal current collectors) are compared to simulated data from the model. Whereas the trend is reproduced, a systematic offset of 100 mV was evident. This can be attributed partly to the back diffusion and mainly to the non-negligible electronic conduction of the thin zirconia electrolyte used in the stacks, causing a leakage current and drop in open circuit voltage (OCV). Correcting for these factors, experimental results at different flux conditions were accurately reproduced by the model (see Fig 7).

2.3 State-Space Modeling of electrochemical reactions

2.3.1 Model Considerations

In State-Space Modeling (SSM), the faradaic impedance of electrochemical reactions is calculated by numerical assessment of the transfer function of single-input single-output systems using modern and user-friendly computational tools. A general framework of this approach was presented by Mitterdorfer and Gauckler [9,10] as well as by Gabrielli and Tribollet [26]. In the time domain, the SSM of a given reaction is written as:

$$\dot{\boldsymbol{x}}(t,\boldsymbol{p}) = d\boldsymbol{x}(t,\boldsymbol{p})/dt = f\left(\boldsymbol{x}(t,\boldsymbol{p}), E(t), t, \boldsymbol{p}\right) \tag{2}$$

$$I_F(t,\boldsymbol{p}) = g\left(\boldsymbol{x}(t,\boldsymbol{p}), E(t), t, \boldsymbol{p}\right), \tag{3}$$

with $\boldsymbol{x}$ being the vector of the state variables (typically the concentration of the intermediate species involved in the reaction mechanism), E the potential, I_F the faradaic current, t the time and $\boldsymbol{p}$ the vector of the model parameters (notably the model rate constants). Under steady-state conditions and with the assumption that a small amplitude sinusoidal perturbation is applied to the potential E, the governing equations are linearized und subsequently Laplace-transformed. In the frequency domain, this leads to:

$$Y_F(j\omega,\boldsymbol{p}) = Z_F(j\omega,\boldsymbol{p})^{-1} = \mathbf{C}(j\omega\,\mathbf{I}-\mathbf{A})^{-1}\mathbf{B}+\mathbf{D}, \tag{4}$$

where _ is the angular frequency, Y_F the faradaic admittance transfer function, Z_F the faradaic impedance, **I** the identity matrix and **A**, **B**, **C** and **D** the state-space matrices calculated from the linearization.

2.3.2 Application to SOFC

Mitterdorfer and Gauckler [9,10] developed the framework of modern SSM calculations and investigated the faradaic impedance of the $Pt,O_2|YSZ$ system. Bieberle and Gauckler [11] studied the $Ni,H_2\text{-}H_2O|YSZ$ interface by combining SSM and the use of geometrically well-defined electrodes, as further explained in Section 2.3.3. Current research focuses on systems of higher complexity and notably on oxygen reduction at mixed ionic-electronic conductors (MIEC), where surface and bulk pathways are parallel as shown in Fig. 8. MIEC are promising candidates for intermediate temperature SOFC, however, the mechanism of oxygen reduction is not clearly understood and subject to controversy [27-29]. Still, the identification of the main reaction pathway is crucial for the design of electrodes with reduced electrokinetic losses. If the reaction follows predominantly the surface pathway, porous electrodes promoting charge transfer at the triple phase boundary (*tpb*) gas/electrode/electrolyte are desired. In contrast, if the bulk pathway is rate-determining, thin dense electrodes should be considered. The implementation of such reaction models can be conveniently carried out within the framework of SSM. Impedance spectra as well as steady-state polarization curves can be calculated as a function of the rate determining steps and compared with experimental data in order to identify the governing reaction pathway. A theoretical study of the surface pathway is reported by Prestat and Gauckler [30] and is illustrated in Fig. 9.

2.3.3 Outlook of SSM in SOFC

The reaction models evaluated with SSM are validated or rejected by comparing simulations against experiments. For this purpose, it is possible to use conventional SOFC electrodes with porous structure. Nevertheless, there has been a recent but continuously increasing interest in academic research for geometrically well-defined (*gwd*) electrodes. These electrodes control the dimensions of the regions where chemical and electrochemical reactions occur [11,30]. The combination of SSM with *gwd* electrodes opens new and

promising perspectives for the comprehension of reaction mechanisms. A first step in this direction was reported recently [11]: nickel pattern electrodes prepared by sputtering and photolithography were used to study the influence of the *tpb* length on the kinetics of hydrogen oxidation. Another application of SSM is the investigation of the competition between bulk and reaction pathways in MIEC, as illustrated in Fig. 8. The kinetics of the surface pathway is strongly dependent on the length of the *tpb*, whereas the surface area and the thickness of the electrode influence the rate of the bulk pathway. Investigations on oxygen reduction at thin dense mixed conducting $La_{0.6}Sr_{0.4}Co_{0.2}Fe_{0.8}O_{3-\delta}$ films are under progress at ETH-Zurich.

So far, only half-cells have been studied with SSM. The next advance in theoretical understanding will consist of complete SOFC modeling. In this context, one topic of particular interest is the so-called single chamber SOFC [31,32]. This remarkable type of SOFC exhibits significant voltage and current densities even though the cathode and anode are exposed to the same atmosphere. The concept of reaction-selective electrodes, wherein this peculiar behavior originates, is still under question. Decisive information concerning the mechanisms and kinetics of such reactions could be obtained with SSM.

2.3.4 Application to PEFC

SSM was employed to study the carbon monoxide (CO) catalyst poisoning kinetics in the Pt anode electrode of a PEFC. It is well-known that even very small concentrations of CO in the fuel (in the order of 10-100 ppm) may strongly increase the anode overpotential at a specific current density of the fuel cell. Hence, a quantitative assessment of CO poisoning is of the utmost importance for fuel cell development. Although the electro-oxidation reaction of CO on Pt in acidic electrolyte has been subject of intensive studies over many years, a detailed understanding of the fundamental processes is still lacking [12]. A purely kinetic model of the anode reactions was employed. There is a general consensus that apart from the slow desorption process, CO may be electro-catalytically removed by reacting with OH as to release free catalyst sites for the hydrogen oxidation reaction (HOR). The OH itself is formed on the catalyst surface by water splitting. Hence, in a purely kinetic approach, the fuel cell anode reactions can be formulated as follows:

$$H_2 \; ? \; ?^{k_{ad}^H} \blacklozenge \; 2(Pt - H_{ad}) \qquad (5)$$

$$2(Pt - H_{ad}) \; ? \; ?^{k_r^H} \blacklozenge \; 2H^+ + 2Pt + 2e^- \qquad (6)$$

$$H_2O + Pt\Re ?^{K_{OH}} ? \blacklozenge \; Pt - OH_{ad} + H^+ + e^- \qquad (7)$$

$$CO + Pt\Re ?^{K_{CO}} ? \blacklozenge \; Pt - CO_{ad} \qquad (8)$$

$$Pt - CO_{ad} + Pt - OH_{ad} \; ? \; ?^{k_r^{CO}} ? \blacklozenge \; CO_2 + 2Pt + H^+ + e^- \qquad (9)$$

k_{ad}^H and k_r^H are the adsorption and the reaction rate coefficient of hydrogen, respectively; $K_{CO} = k_{ad}^{CO}/k_{des}^{CO}$ and k_r^{CO} denote the equilibrium constant of the CO adsorption/desorption and the oxidation rate of CO_{ad}, respectively, and K_{OH} is the equilibrium constant for OH formation. It is further assumed that the CO adsorption is governed by a Frumkin-isotherm, considering the adsorbent-adsorbent interactions of CO. The impedance contributions arising from mass transport limitations are neglected, the reason being that the relaxation time for spherical diffusion from the bulk is likely to be short to interfere with the processes discussed here.

The SSM approach was used to rationalize the theoretical impedance response of the employed model. The state equations (Eqs. (2)), adapted to express the mass balance on the catalyst surface are as follows:

$$d\grave{e}_i/dt = f_i\left(k_{ad}^i, k_{des}^i, k_r^i, \ldots, \grave{e}_i, \varsigma_j\right), \qquad (10)$$

with η the electrode overpotential. In terms of the H_{ad}, CO_{ad} and OH_{ad} coverage, Eq. (10) yields:

$$\beta\frac{d\theta_H}{dt} = v_{ad}^H - v_{des}^H - v_r^H, \quad \beta\frac{d\theta_{CO}}{dt} = v_{ad}^{CO} - v_{des}^{CO} - v_r^{CO},$$

$$\text{and } \beta\frac{d\theta_{OH}}{dt} = v_f^{OH} - v_b^{OH} - v_r^{CO} \qquad . \qquad (11)$$

The rates in Eq. (11) are: $v_{ad}^H = k_{ad}^H x_H P_A \theta_0^2$, $v_{des}^H = b_{des}^H k_{ad}^H \theta_H^{\;2}$, $v_r^H = 2\theta_H k_r^H \sinh(\eta_H/b_H)$ for H_2, $v_{ad}^{CO} = k_{ad}^{CO} x_{CO} P_A e^{-g\theta_{co}} \theta_0$, $v_{des}^{CO} = b_{des}^{CO} k_{ad}^{CO} \theta_{CO} e^{g\theta_{co}}$, $v_r^{CO} = k_r^{CO} \theta_{CO} \theta_{OH} e^{\eta_{CO}/b_{CO}}$ for

CO and $v_f^{OH} = k_f^{OH}\theta_0 e^{\eta_{OH}/b_{OH}}$, $v_b^{OH} = k_b^{OH}\theta_{OH} e^{-\eta_{OH}/b_{OH}}$ for OH; β denotes the charge required for complete hydrogen adsorption, b_i the Tafel slopes for the individual charge transfer processes, P_A the pressure, and $\theta_0 = 1-\theta_H-\theta_{CO}-\theta_{OH}$ the fraction of uncovered sites. The faradaic current is obtained from Eq. (3):

$$I_F = g\left(k_r^I,\ldots,\theta_i,\eta_i\right) = v_r^{II} + v_r^{CO} + v_f^{OH} - v_b^{OH} \tag{12}$$

For the electrode overpotential, it is assumed that $\eta = \eta_H = \eta_{CO} = \eta_{OH}$ [33]. The impedance function due to the faradaic current, Z_F, is given in Eq. (4). The total anode impedance Z is:

$$Z = (Z_{dl}^{-1} + Z_F^{-1})^{-1}\ , \tag{13}$$

considering also the double layer impedance Z_{dl}. In Eq. (4), $\mathbf{A}_{ij} = ff_i/f\theta_j$ is the Jacobian matrix of the state equation vector field f, $\mathbf{B}_i = ff_i/f\eta$, $\mathbf{C}_j = fg/f\theta_j$ are vectors and $\mathbf{D} = fg/f\eta$ is a scalar.

Typical computed spectra of the impedance function are given in Figs. 10 and 11 as a function of the applied overpotential η. The system parameters for those simulations were taken from the literature [34]. With increasing overpotential, the spectra in the Nyquist plot of Fig. 10 change from two capacitive arcs ($\mathrm{Im}(Z) < 0$) to a superposition of a capacitive high frequency (*hf*) and an inductive ($\mathrm{Im}(Z) > 0$) low frequency (*lf*) arc. The Bode plot of Fig. 11 reveals that the phase angle of the slow process changes sign above $\eta \approx 0.2$, whereas the fast process remains capacitive. The same tendency was also observed in experiments: cells undergoing only a weak CO poisoning (accompanied with a small cell voltage drop) show purely capacitive arcs in their impedance spectra. Strongly poisoned cells, on the other hand, have typical spectra with an inductive low frequency end [12].

The effect of poisoning is characterized by the system parameters (CO adsorption, CO desorption, OH formation rates etc.), which in turn depend mainly on the catalyst material and temperature. In literature, the shift from capacitive to inductive low frequency behavior has been attributed to the onset of CO electro-oxidation [35] (since it was assumed that all electrochemical reactions have the same equilibrium potential, the CO electro-oxidation actually occurs for all $\eta > 0$). However, this shift is in fact the result of

the interaction between Z_F and Z_{dl} [33]. Consider, for example, the simplified case where only one state variable θ ($\theta = \theta_{CO}$) is accounted for. Then, Y_F in Eq. (4) simplifies to $Y_F = \mathbf{C}(j\omega\mathbf{I} - \mathbf{A})^{-1}\mathbf{B} = CB/(j\omega - A)$, where $A < 0$ and B, $C > 0$ are scalars. Hence, Z_F may be thought to be an inductance $L = (CB)^{-1}$ in series with a resistance $R_0 = A?(CB)^{-1}$, both parallel to the charge transfer resistance D [33,36]. Then, depending on the values of the double layer capacitance (C_{dl}) and L and R_0, inductive behavior can be observed [37]. High values of L^{-1} and low values of A favor inductive *If* behavior.

If a high overpotential is required for a chosen current density (strong CO-poisoning), then $B = f\dot{\theta}/f\eta$ and $A = f\dot{\theta}/f\theta$ tend to increase and decrease, respectively, ($C = fI_F/f\theta$ is governed by the HOR current and may be considered independent of the catalyst's CO tolerance at a first approximation). Hence, a strong CO poisoning favors the appearance of an *If* inductive arc in the spectra, as also observed in experiments. Additionally, a high C_{dl} (a neutral, in terms of CO poisoning, materials constant) favors a capacitive *If* end. A high C_{dl} may help discriminating the cathodic charge transfer impedance from the impedance due to CO poisoning, when the effect of CO on the fuel cell performance is less pronounced [37].

2.4 Lattice Boltzmann Modeling

Essential advantages of the Lattice Boltzmann (LB) method are the simple underlying algorithm, allowing parallel computer implementation, intrinsic stability and capability to deal with arbitrarily shaped geometrical boundaries. A prerequisite for the application of the method is the extensive use of automatically generated computational Lattice meshes representing the porous structure under consideration. Fuel cell electrodes and supports are characterized by a wide range of potential material structures, such as isotropic material of random porous structure, metallic and ceramic foams, textile structures and highly anisotropic structures consisting of needle-like components. Typical PEFC porous electrode materials are illustrated in Fig. 12. The characterization of porous fuel cell electrodes and their reconstruction for computer simulations is presented next.

2.4.1 *Hybrid reconstruction of isotropic material structures*

The material characterization starts with the digitization of 2-D material slices utilizing a so-called "krigging" algorithm [38] for two passes over the grey level image of the computer tomography (CT) picture. In the first pass, an a-priori population assignment is done based upon a threshholding window. In the second pass, the reminder of the population assignment is obtained by indicator krigging. Finally, an eroding step is applied. Statistical properties [39] such as the Two-Point Correlation Function $F(r)$, the Lineal-Path-Function $L(r)$, which is the probability to find a line segment of length r that lies entirely in the pore space, and the Cord-Length-Function $C(r)$ (the probability of finding a line segment of length r that lies in the pore space and touches the solid on both sides) can be derived from a digitized 2-D slice. To generate an artificial material slice with the same correlation functions as the 2-D digitized image (reference slice), the energy function, which is the summed squared difference between the statistical functions of the reference slice and a randomly initialized slice, have to be minimized. Starting from a randomized generated initial guess, which has the same porosity as the reference slice, pixels are interchanged. The interchange of the pixels is accepted if the energy function decreases. This is done by using the Metropolis *et al.* [40] algorithm, until a minimum of the energy function is reached. The above mentioned statistical functions can be easily expanded to 3-D material reconstruction. Figure 13 illustrates the 3-D reconstruction based on a 2-D digitized slice of Fig. 12b.

2.4.2 *Overlapping spheres model (OSM) of foam structures*

The overlapping spheres model is the combination of a pore-finding algorithm and a Boolean model using spherical subsets; as such, it is well-suited for the generation of foam structures. As before, digitized 2-D CT images are used to derive pore size and distance distributions. The method to reconstruct the porous medium can be divided into two basic steps, as shown in Fig. 14. The first step locates disc centers within the reference slice using the "skeleton" algorithm [41]. The skeleton algorithm itself utilizes the Euclidean distance map of the slice [42]. It usually finds more disc centers than those required for reconstruction. The reduction of disc centers is done by placing discs of maximum diameter around the centers and deleting the centers of fully overlapping discs. The second

step involves the determination of the pore radii distribution, based on the radii derived by the application of the above algorithm. The solution of the Goldsmith integral equation provides the pore radius distribution [43,44]. Additionally, the number of pores per specific area can be determined and used to parameterize a Poisson distribution.

2.4.3 Reconstruction of Non-Isotropic Material Structures

Fuel cell electrodes can exhibit highly anisotropic material characteristics. In this case alternative methods should be sought for their computer representation. For such material structures, parameterization of the base geometry is considered to be the most effective way. The base geometry, for example, in a textile structure is represented by a simple curved tube segment of given diameter and bending radius. By connecting a number of these base segments together, the surface of a material sample can be formed. Thus, only two parameters (diameter and bending radius of the textile fibre) are sufficient to characterize the surface. This surface is then used to generate the computational mesh within a small portion of the flow domain. Since the LB method uses strictly regular equidistant computational meshes, the curved material surface in the computer model is always approximated by "stair cases". It is hence evident that the accuracy of resolution of the material structure is directly linked to the computational mesh density.

2.4.4 Outlook for fuel cell applications

Recent comparisons [15] between measured and predicted pressure drop in a real porous structure with an artificially generated geometry using the approach described above and the corresponding LB-based flow predictions, showed excellent agreement. In addition, a 2-D LB model has been applied to simulate half the PEFC domain (porous cathod diffusion layer and channel flow); preliminary comparisons between measured and predicted production of H_2O and consumption of O_2 were in good agreement to each other.

2.5 Three-dimensional modeling and thermodynamic optimization of FC

The previous approaches have utilized a lower-dimensionality approach (mostly 2-D). The current approach aims at introducing a full 3-D description in PEFC. The three-dimensionality arises when gradients in all directions become important. The entire

process is after all three dimensional. Three-dimensional computational modeling provides an improved understanding of the fundamental transport phenomena inside the fuel cell and therefore allows for efficient, scientifically-based thermodynamic optimization, which aids significantly the design of PEFC. Moreover, 3-D modeling is crucial in capturing performance-limiting effects such as mass transfer limitations to and from the portion of the diffusion layer that is not covered by flow channels as well as ohmic losses due to electron and proton transport in the MEA.

For this purpose, a 3-D model [17,18] has been defined at the Laboratory of Thermodynamics in Emerging Technologies of ETHZ. The model is based on the formulation of the Navier-Stokes equations, the energy equation, the species conservation equations, and the electric current conservation equations. It accounts for the finite thickness of the catalyst layers as well as of the membrane and the governing equations inside each of these layers are solved in three dimensions. Two different electric potential fields are considered, i.e. a solid potential field governing the transport of electrons and a membrane potential field governing the transport of protons. Rates of electrochemical reactions in the catalyst layers are described by Butler-Volmer equations. The set of coupled nonlinear differential equations is solved numerically using the finite volume method on a structured or unstructured grid.

Computational modeling provides a more fundamental understanding of the physical phenomena occurring inside a thermodynamic system and, moreover, forms the basis of thermodynamic optimization. Entropy generation minimization [45] subject to physical constraints, that are responsible for the irreversible operation of a device, is the method of modeling and optimization of real devices for which the thermodynamic imperfection is due to heat transfer, mass transfer, and fluid flow irreversibilities. Entropy generation minimization is also known as "thermodynamic optimization" and "finite time thermodynamics" in the engineering and physics literature, respectively. A wide range of fuel cell models of different sophistication levels are available in the literature, targeting at improving the scientific understanding of the fundamental processes, while only a limited number of studies are dedicated to advanced thermodynamic optimization.

The full 3-D model of the entire cell is under development, however, initial results for optimized FC flow distributors and porous materials are presented below.

2.5.1 Porous materials as fluid distributors

It is particular to fuel cells with ribbed flow distributors, that the diffusion paths for reactant and product molecules between the channel and the catalyst layer are not constant. The mass transfer rate to and from the reacting zones under the current collector shoulders is reduced compared to the mass transfer rate to zones under the flow channels, due to longer diffusion paths. This phenomenon is most prominent on the cathode side of fuel cells operated with air and hydrogen due to the low diffusivity of oxygen in nitrogen. The limitations on the cathode side manifest themselves in reduced oxygen mole fractions and increased water vapor mole fractions under the current collector shoulders, as shown in Fig. 15. Removal of water vapor from these regions is also limited. As a result, a higher saturation level is observed under the shoulders. The drawback of mass transfer non-uniformity can be eliminated by replacing the traditional ribbed flow distributors with distributors made out of a porous medium [17,18], since the diffusion layers are continuously covered with the bulk flow through the permeable porous matrix. Therefore, the oxygen mole fraction and all other quantities vary in the flow direction only and not in the lateral direction.

2.5.2 Tree network channels as fluid distributors resulting in pyramidal shaped fuel cells

Constructal tree network channels [46] have been recently introduced by Senn and Poulikakos [47,48] as a novel fluid distribution concept in PEFC [47] and direct methanol fuel cells [48]. Two-dimensional along-the-channel models derived from first principles are developed to accurately predict the polarization curves of fuel cells with tree network fluid distributors. The entire geometric structure of the fluid distribution system has been optimized with respect to maximum electric power densities and maximum net power densities, subject to the constraint of a fixed cell area, resulting in an optimum "pyramidal" or "double staircase" shaped tree network (see Fig. 16) that is based on the functionality of the fluid distribution system, in contrast to the traditional rectangular shapes of fuel cells. In this context, a net power density is defined as the difference between the electric power

density and the pumping power density required for the fluid circulation. Multiobjective genetic search is performed for optimization in terms of constructal parameters and operating conditions. As a result of their intrinsic advantage with respect to both mass transfer and pressure drop, tree network channels can provide substantially improved electric and net power densities compared to the traditional non-bifurcating serpentine channels. Tree network channels for thermal management in PEFC have been investigated numerically [49] to gain a more detailed understanding of the fundamental 3-D heat transfer and fluid mechanics phenomena.

2.5.3. Optimal hydrocarbon reformer design for micro SOFC applications

The optimization of a fuel reformer for a micro fuel cell unit based on catalytic partial oxidation is studied using a systematic numerical investigation of chemical composition and inflow conditions. The optimization targets hydrogen production from methane. The operating temperature, the amount of carbon formation and the methane conversion efficiency are further considered. The fundamental investigation is based on simplified reactor models (surface perfectly stirred reactor), which consider the process residence time. A detailed surface chemistry mechanism is adopted in order to capture all the important features of the reforming process. In order to ensure the validity of the findings from the simplified reactor model, more elaborate simulations (involving the Navier-Stokes equations) are performed for the regions of interest. An optimal operation region, where all the targeted operating conditions are satisfied and the hydrogen yield is around 80% is identified [50].

2.5.4. SOFC with internal steam reforming

From the points of view of infrastructure, cost and efficiency, SOFCs operating under internal reforming of natural gas (95% methane) constitute a very attractive solution. To study the replacement of H_2 to CH_4 on SOFC, the repeat element of the HTceramix design [7] was modeled in 3-D with the CFD code Fluent [16], computing the coupled phenomena of heat transfer (conduction/convection/radiation), multi-component gas flow (concentration, velocity and pressure fields, including diffusion), electrochemical reactions (local temperature, ionic current and electronic leakage current) and steam reforming

kinetics. The comparison is illustrated in Fig. 17 for a H_2-fed cell and for a CH_4-fed cell where the methane is 50% pre-reformed with a steam-to-carbon ratio of 2.5. The cell is operated at 0.6 V in an 800°C furnace. Strong differences in the temperature fields are observed, with the advantage of partial stack temperature control given by internal reforming cooling near the fuel entrance; when using H_2, the temperature is the highest at the fuel entry position.

2.5.5 Thermo-economic modelling and optimization of fuel cell systems

The goal of the presented methodology for integrating and optimizing fuel cell systems is to help in the design step. The thermo-economic model developed includes three parts: a) the energy flow model that represents the thermodynamic performances of the chemical and energy conversions considered in the system; b) the model of heat transfer based on process integration [51], and c) an economic module that estimates cost of each of the devices considered in the system. The method uses a superstructure that includes the major options to be considered for the energy conversion in the system. A multi-objective optimization approach [19] based on evolutionary algorithms is used to extract from the superstructure the most promising configurations and compute for each of them the best operating conditions. The objectives considered are minimal specific cost of electricity production and maximal system efficiency. The proposed method is generic and may be applied to different types of fuel cell systems. The results of the thermo-economic optimization of a PEFC system have shown [19] that at higher cost and higher efficiency steam reforming is preferred, whereas at lower cost but lower efficiency autothermal reforming is favored. In all the cases, the single medium temperature WGS (water gas shift) reactor is chosen for its lower cost.

3. Conclusions

The modeling and simulations constitute an ever increasing part of the entire FC research program. Taking into account the predominant transport direction(s) in large cells, models with reduced spatial dimensionality and very high computational efficiency have been developed, particularly suited for global performance prediction and engineering design. Such models included the (1+1) dimensionality approach, which decoupled the in-plane and through-plane processes, and the volume-averaged approach that considered only the lumped effect of certain pre-selected system components. The former reproduced well the measured lateral current density inhomogeneities (a key design issue) in a PEFC and the latter provided an optimization tool for the Sulzer HEXIS SOFC and for the HTceramix SOFC stack.

The details of the electrochemical reactions have been elucidated with State Space Modeling (SSM). SSM has been used to identify the main reaction pathways in SOFC systems and, in conjunction with the implementation of geometrically well-defined (*gwd*) electrodes, has opened a new direction for the understanding of reaction mechanisms. Furthermore, the SSM investigation of the CO poisoning kinetics in the Pt anode electrode of a PEFC has aided the understanding of the relative contributions to the CO-poisoning-induced anode impedance.

Models for entire cells and stacks that retain a fundamental level description are currently under development. The Lattice Boltzmann (LB) method provides a good alternative for the transport in mesoscopic structures such as the porous electrode materials of PEFC. Within this framework, a technique for the characterization and computer-reconstruction of the porous electrode structure was developed using advanced pattern recognition algorithms; the ultimate goal is to couple the technique with detailed LB transport simulations (2-D or 3-D) in a fuel cell. In the direction of thorough CFD modeling, new efforts were reported for full 3-D simulations; modeling of selected components as well as the entire fuel cell unit has underpinned the significance of porous and novel fractal channel distributors for the fuel and oxidant delivery, as well as for the cooling of PEFC. In addition, results to date for the entirely new concept of functionally

optimized fractal-shaped fuel cells (not only flow distributors), shows promise of significant performance improvements over the conventional rectangular shaped units.

Thermo-economic modeling was finally applied in PEFC to identify most promising configurations and optimum operating conditions as to minimize the specific cost of electricity production and maximize the system efficiency.

4. Acknowledgements

The help of Dr. Marco Stampanoni from the Swiss Light Source (SLS) of PSI in providing beamtime for the computer tomography experiments of PEFC electrodes is appreciated. BfE (program manager Dr. A. Hintermann) provided financial support to the Center for Computational Physics (ZHW), the Laboratory of Thermodynamics in Emerging Technologies (LTNT) and the Laboratory of Industrial Energy Systems (LENI). L.J. Gauckler, M. Prestat and B. Andreaus thank ETH-Zürich. LENI further acknowledges the support of the Swiss National Science Foundation and the Swiss Commission for Technology and Innovation.

5. References

[1] S. Dutta, S. Shimpalee, J. VanZee, *J. Appl. Electrochem.* **2000**, *30*, 135.

[2] S.A. Freunberger, 'Wasserhaushalt und Leistungsverhalten von Polymer-Electrolyt Brennstoffzellen technischer Relevanz', Diploma Thesis, Paul Scherrer Institut, Switzerland and TU Vienna, Austria, **2002**.

[3] A.A. Kulikowski, *Electrochim. Acta* **2004**, *49*, 617.

[4] G.J.M. Janssen, *J. Electrochem. Soc.* **2001**, *148*, A1313.

[5] M. Roos, E. Batawi, U. Harnisch, T. Hocker, *J. Power Sources* **2003**, *118*, 86.

[6] U. Harnisch, M. Roos, E. Batawi, T. Baumgartner, A. Schuler, 'Numerical Simulation of HEXIS-SOFC Systems', Proceedings of the fifth European SOFC Forum, Luzern, **2002**, p. 953.

[7] D. Larrain, J. Van herle, F. Maréchal, D. Favrat, *J. Power Sources* **2004**, *131*, 304.

[8] J.R. Macdonald, 'Impedance Spectroscopy', John Wiley & Sons, New York, **1987**.

[9] A. Mitterdorfer, L.J. Gauckler, *Solid State Ionics* **1999**, *117*, 187.

[10] A. Mitterdorfer, L.J. Gauckler, *Solid State Ionics* **1999**, *117*, 203.

[11] A. Bieberle, L.J. Gauckler, *Solid State Ionics* **2002**, *23*, 146.

[12] F. Hajbolouri, 'Polymer Electrolyte Fuel Cells: Contributions to the Understanding of CO-Tolerance', ETH-Dissertation Nr. 15525, **2004**.

[13] S. Chen, G.D. Doolen, *Ann. Rev. Fluid Mech.* **1998**, *30*, 329.

[14] J. Steiner, C. Redl, W. Brandstätter, A. Triesnig, 'Simulation of Bubble Formation Based on the Lattice Boltzmann Method', TMS Conference Proceeding, Charlotte, North Carolina, **2004**.

[15] S. Salchenegger, W. Brandstätter, B. Andreaus, G. Scherer, 'A 1-Dimensional Computational Model to Study Dehydration Phenomena in Polymer Electrolyte Fuel Cells', France-Deutschland Fuel Cell Conference on Materials, Engineering, Systems, and Applications, **2002**.

[16] N. Autissier, D. Larrain, J. Van herle, D. Favrat, *J. Power Sources* **2004**, *131*, 313.

[17] S.M. Senn, D. Poulikakos, 'Porous Materials as Fluid Distributors in Polymer Electrolyte Fuel Cells - Computational Performance Analysis', IMECE 2003-42310, ASME Int. Mechanical Eng. Congress and Exposition, Washington D.C., **2003**, p. 1.

[18] S.M. Senn, D. Poulikakos, *J. Heat Transfer-Transactions ASME* **2004**, *126*, 410.

[19] G.B. Leyland, 'Multi-Objective Optimisation Applied to Industrial Energy Problems', EPFL-Dissertation Nr. 2572, **2002**.

[20] S. Whitaker, 'The Method of Volume Averaging', Kluwer Academic Publishers, Dordrecht, The Netherlands, **1999**.

[21] A.Z. Weber, J. Newman, *J. Elect. Chem. Soc.* **2004**, *151*, A327.

[22] E. Anderheggen, J.G. Korvink, M. Roos, G. Sartoris, H.U. Schwarzenbach, NM SESES user manual, download at: www.nmtec.ch, **2004**.

[23] T. Hocker, E. Heinzelmann, *Technische Rundschau* **2004**, *5*, 22.

[24] P. Held, T. Hocker, J. Frei, J. Hoffmann, 'Numerical Analysis of Critical Performance Parameters of the Sulzer Hexis SOFC Stack', Lucerne Fuel Cell Forum, **2004**, submitted.

[25] C.C. Pantelides, P.I. Barton, *Comp. Chem. Eng.* **1993**, *17S*, S263.

[26] C. Gabrielli, B. Tribollet, *J. Electrochem. Soc.* **1994**, *141*, 1147.

[27] S.B. Adler, J.A. Lane, B.C.H. Steele, *J. Electrochem. Soc.* **1996**, *143*, 3554.

[28] M. Liu, J. Winnick, *Solid-State Ionics* **1999**, *118*, 11.

[29] G.W. Coffey, L.R. Pederson and P.C. Rieke, *J. Electrochem. Soc.* **2003**, *150*, A1139.

[30] M. Prestat, L.J. Gauckler, *J. Electrochem. Soc.* **2004**, submitted.

[31] I. Riess, P.J. van der Put, J. Schoonman, *Solid State Ionics* **1995**, *82*, 1.

[32] B.E. Buergler, M. Siegrist and L.J. Gauckler, Proceedings of the 6th European Solid Oxide Forum, Ed. M. Mogensen, **2004**, submitted.

[33] B. Andreaus, 'Die Polymer-Elektrolyt Brennstoffzelle: Charakterisierung ausgewählter Phänomene durch elektrochemische Impedanzspektroskopie', EPFL-Dissertation Nr. 2598, **2002**.

[34] J. Zhang, R. Datta, *J. Electrochem. Soc.* **2002**, *149*, A1423.

[35] X. Wang, I.-M. Hsing, Y.-J. Leng, P.-L. Yue, *Electrochim. Acta* **2001**, *46*, 4397.

[36] C.-N. Cao, *Electrochim. Acta* **1990**, *35*, 831.

[37] F. Hajbolouri, B. Andreaus, G.G. Scherer, A. Wokaun, *Fuel Cells* **2004**, accepted.

[38] W. Oh, W.B. Lindquist, *IEEE Trans. on Pattern Analysis and Machine Intelligence* **1999**, *21*, 590.

[39] C.L.Y. Yeoung, S. Torquato, *Physical Review E* **1997**, *57*, 495.

[40] N. Metropolis, A.W. Rosenbluth, M.N. Rosenbluth, A.H. Teller, E. Teller. *J. Chem. Phys.* **1953**, *21*, 1087.

[41] W.P. Choi, K.M. Lam, W.C. Siu, *Pattern Recognition* **2002**, *36*, 721.

[42] I. Ragnemalm, 'The Euclidean Distance Transform', Ph.D. Dissertation, Linköping University, Sweden, **1993**.

[43] P.L. Goldsmith, *Brit. J. Appl. Phys.* **1967**, *18*, 813.

[44] G. Bach, *Zeitschrift für wissenschaftliche Mikroskopie* **1963**, *65*, 285.

[45] A. Bejan, *J. Applied Physics* **1996**, *79*, 1191.

[46] A. Bejan, 'Shape and Structure, from Engineering to Nature', Cambridge University Press, Cambridge, **2000**.

[47] S.M. Senn, D. Poulikakos, *J. Applied Physics* **2004**, *96*, 842.

[48] S.M. Senn, D. Poulikakos, 'Pyramidal Direct Methanol Fuel Cells', *J. of Applied Physics,* under review.

[49] S.M. Senn, D. Poulikakos, *J. Power Sources* **2004**, *130*, 178.

[50] A.K. Chaniotis, D. Poulikakos, 'Partial oxidation methane reforming for fuel cells', *J. Power Sources*, submitted, **2004**.

[51] F.Marechal, B. Kaliventzeff, *Computers Chem. Eng.* **1998**, *22*, S149.

Figure legends

Figure 1: Predicted (using an isothermal model) current density distribution in the provided flow field, obtained with the coupling of four (1+1) sections.

Figure 2: Comparison between predicted and measured current density in the four segments of Fig. 1 as function of air stoichiometry: model isothermal, experiment quasi-isothermal.

Figure 3: Predicted temperature and current density distribution for a single (1+1) section with co-flow of the gases and parallel streaming of coolant (all left to right). Coolant flow: infinitely high (●,●), 0.054 kg/m^{2}s (ᘐ,ᘓ), 0.049 kg/m^{2}s (❑,⬧) and 0.039 kg/m^{2}s (■,□).

Figure 4: Decomposition of a PEFC cell into two separate 2-D domains coupled non-locally by a 1-D approximation of the electrochemical interaction across the MEA. The graph shows two sections of the true structure (top) and the corresponding coupled 2-D simulation domains (bottom).

Figure 5: Predicted locally averaged water concentration (molar fraction) within the cathode and the anode flow field.

Figure 6: Mass fraction and potential distribution across the MEA taken from the 1-D simulation of the electrochemical interaction near the H_2 inlet. The dependence of the electric resistivity on Nafion humidification is reflected in the non-linear potential distribution.

Figure 7: Comparison between experimental and calculated i-V behavior for a SOFC repeat element (1045 K). The fuel is hydrogen.

Figure 8: Schematic representation of the oxygen reduction mechanism at MIEC: cross section of the interface electrode/electrolyte. Surface and bulk reaction pathways are parallel and in competition. On the surface pathway, charge transfer occurs at the triple phase boundary gas/electrode/electrolyte.

Figure 9: Oxygen reduction impedance Z_F for different rate determining steps (*rds*): charge transfer (ct, ◘), adsorption and charge transfer (○), surface diffusion and charge transfer (❐) and adsorption, surface diffusion and charge transfer (●) [30]. The numbers on the impedance spectra indicate the frequency in Hz.

Figure 10: Simulated spectra as a Nyquist plot, Re(Z) vs Im(Z), of an anode impedance Z, when the anode is poisoned by CO. The system parameter values were taken from Ref. [34], where a fuel cell with 5 cm^2 active area was employed.

Figure 11: Phase angle of the anode impedance Z as a function of the potential perturbation frequency and the applied stationary overpotential for system parameter values of Ref. [31]. The low frequency process changes the phase from negative values to positive values (where an inductive arc will appear in a Nyquist plot) above $\eta \approx 0.2$ V.

Figure 12: Examples of PEFC porous electrode materials: (a) textile structure, (b) needle-like structure.

Figure 13: Reconstructed porous cube from the image of Fig. 11b.

Figure 14: Sequence showing the basic steps in applying the Overlapping Spheres Model.

Figure 15: 3-D computations of the transport phenomena in a PEFC with a traditional serpentine flow-field [18]: (a) distribution of the oxygen mole fraction in the middle of the cathode diffusion layer, (b) distribution of the relative humidity in the middle of the cathode diffusion layer.

Figure 16: Geometric structure of a constructal "double staircase" shaped polymer electrolyte fuel cell [49,50]. The dashed lines indicate the boundary of the cell. The black rectangles represent the channels which are arranged in parallel. The channel length L_k and the channel diameter h_k are reduced from one branching level to the next higher, while the number of channels increases.

Figure 17: Temperature fields (K) of repeating unit in a SOFC, fed with (a) pure H_2 fuel and (b) 60% pre-reformed methane [16].

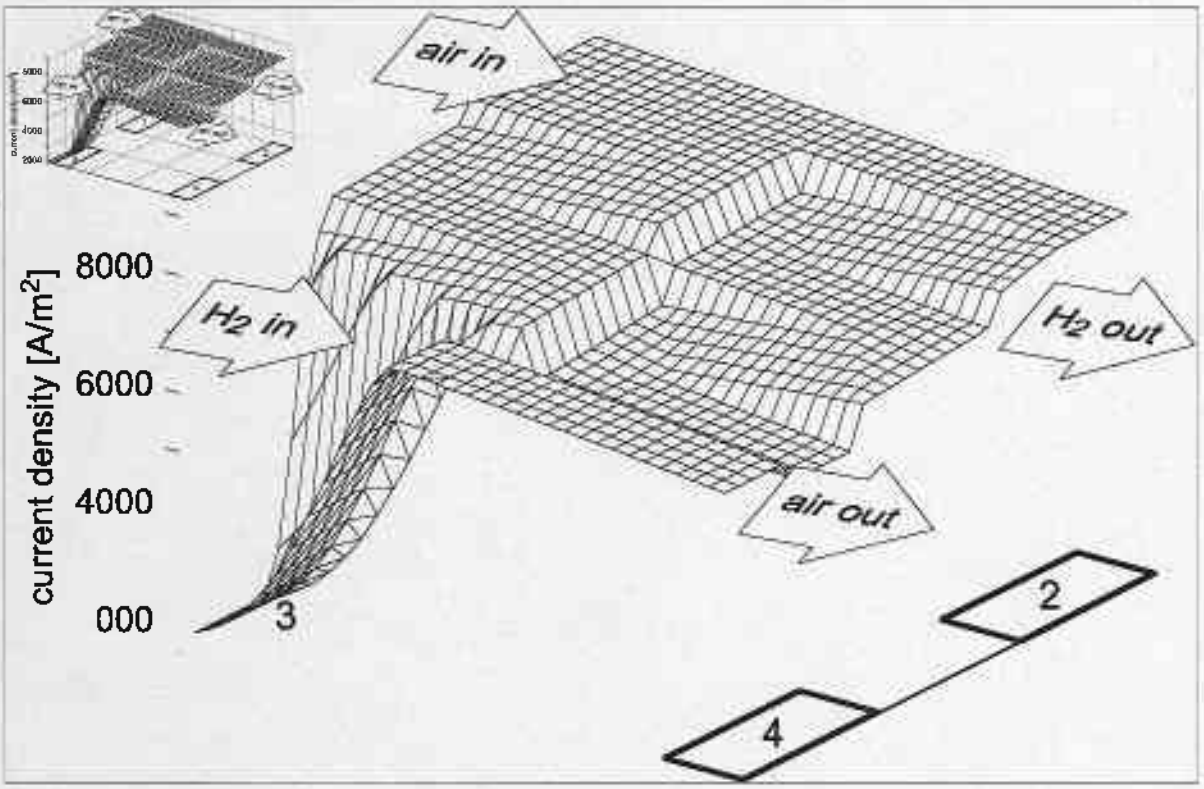
air in
H2 in
H2 out
air out
current density [A/m2]
8000
6000
4000
000
3
2
4

Figure 1

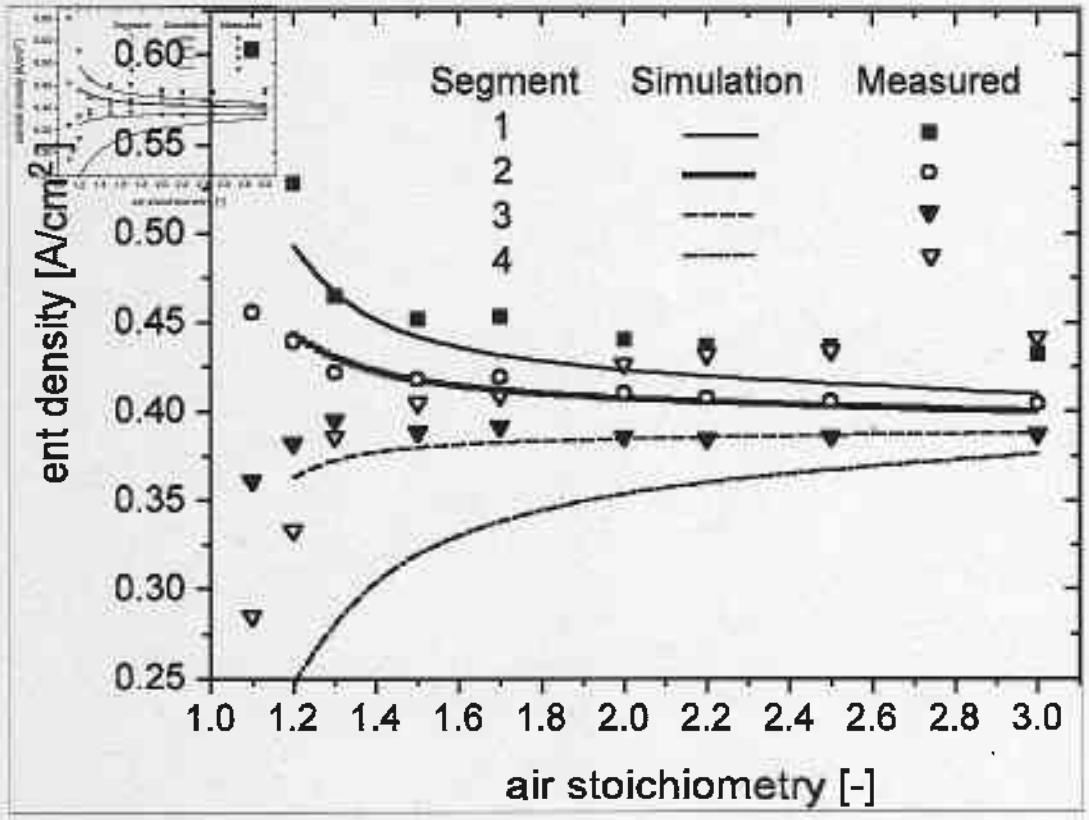
Segment
Simulation
Measured
1
2
3
4
0.60
0.55
0.50
0.45
0.40
0.35
0.30
0.25
ent density [A/cm2]
1.0
1.2
1.4
1.6
1.8
2.0
2.2
2.4
2.6
2.8
3.0
air stoichiometry [-]

Figure 2

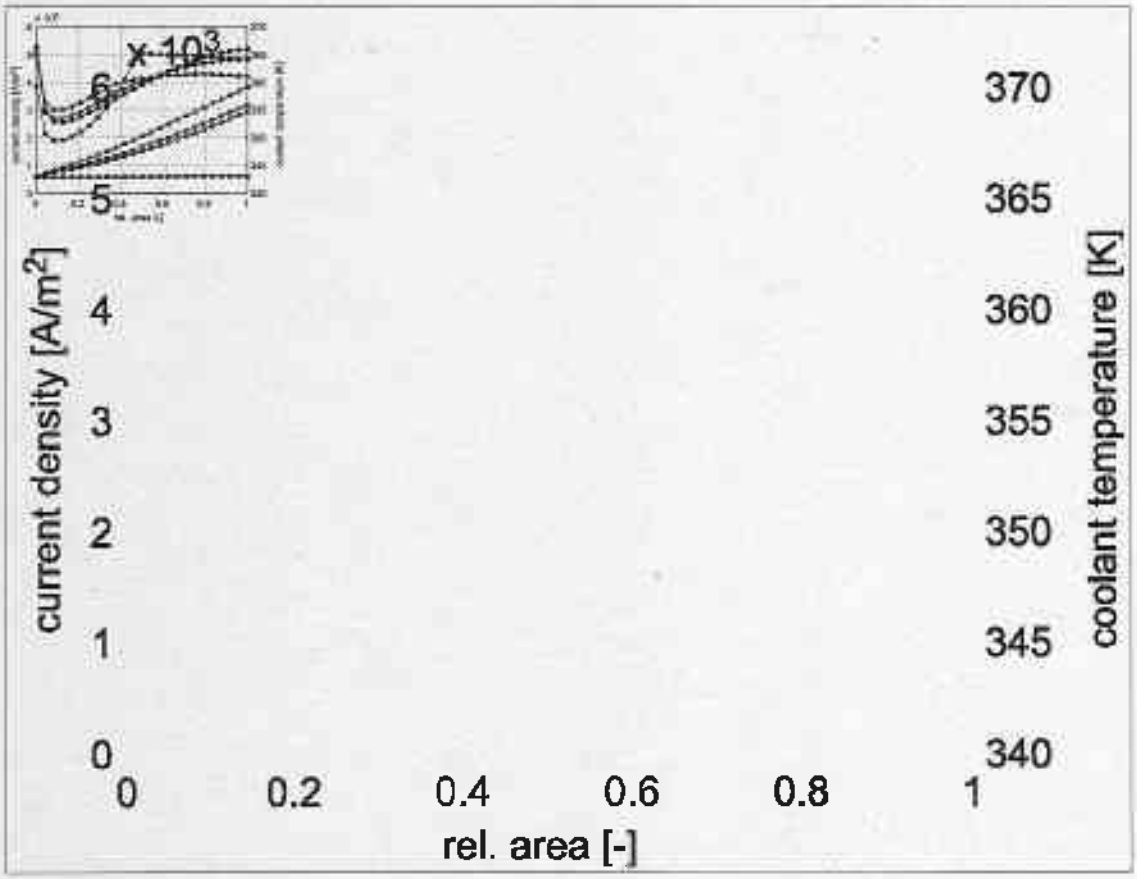
x 10^3
6
5
current density [A/m^2]
4
3
2
1
0
0
0.2
0.4
0.6
0.8
1
rel. area [-]
370
365
360
355
350
345
340
coolant temperature [K]

Figure 3

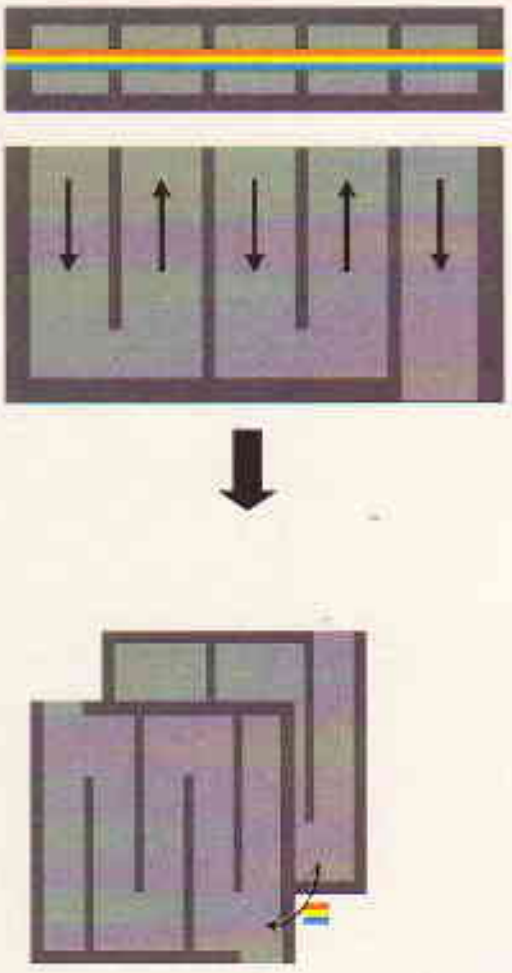

Figure 4

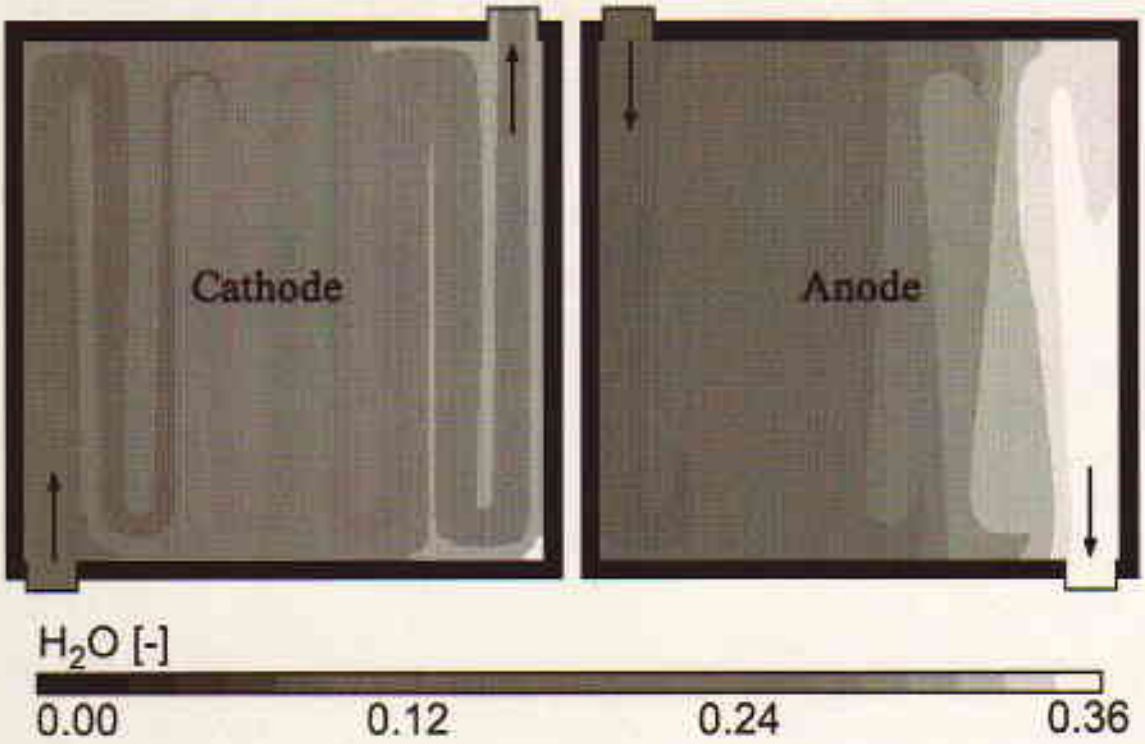

Figure 5

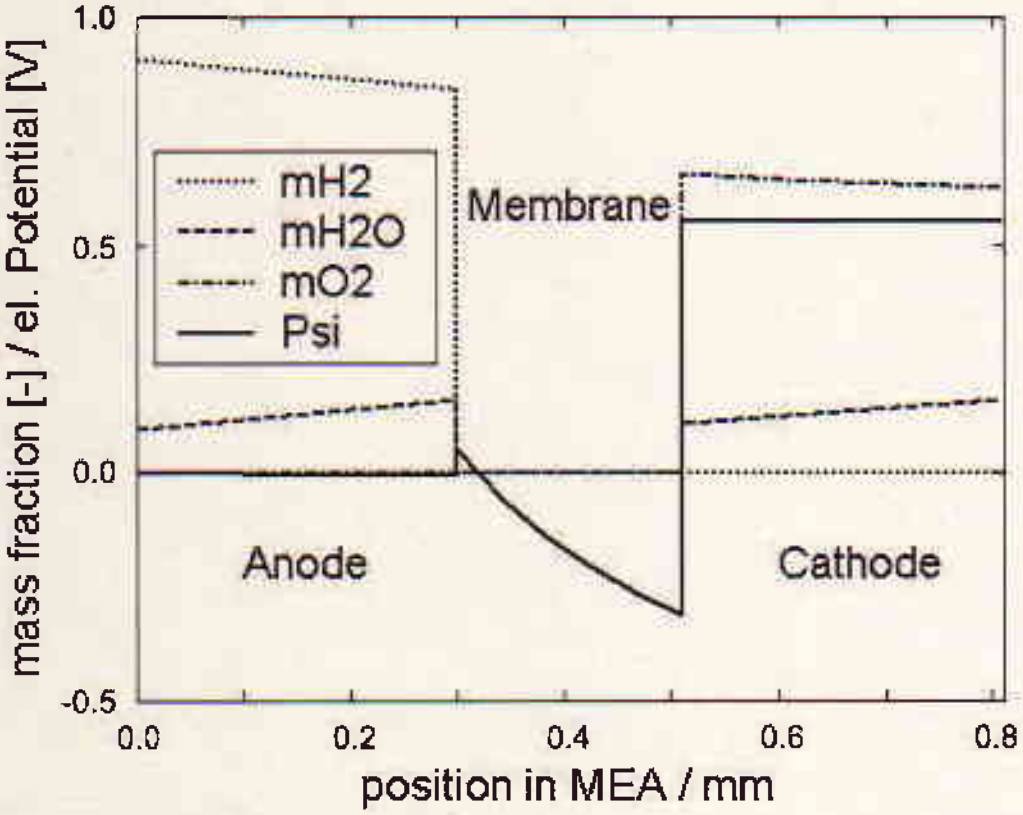
1.0
0.5
0.0
-0.5
mass fraction [-] / el. Potential [V]
mH2
mH2O
mO2
Psi
Membrane
Anode
Cathode
0.0
0.2
0.4
0.6
0.8
position in MEA / mm

Figure 6

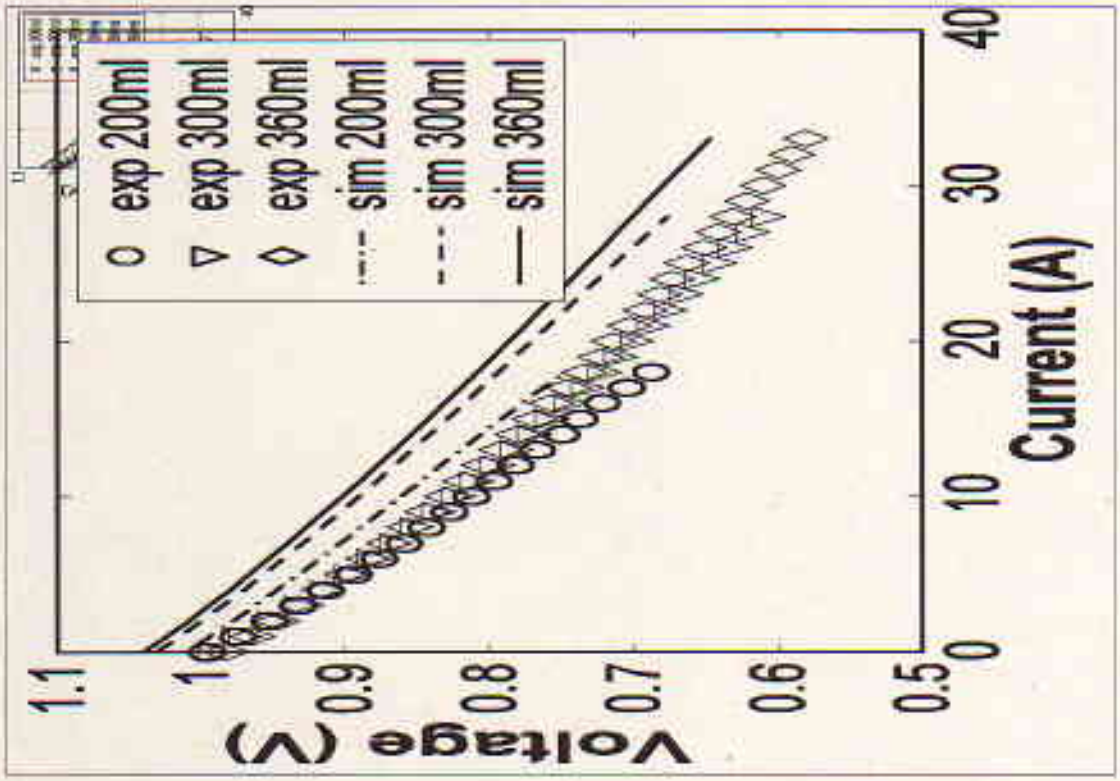
exp 200ml
exp 300ml
exp 360ml
sim 200ml
sim 300ml
sim 360ml
Voltage (V)
Current (A)
1.1
1
0.9
0.8
0.7
0.6
0.5
0
10
20
30
40

Figure 7

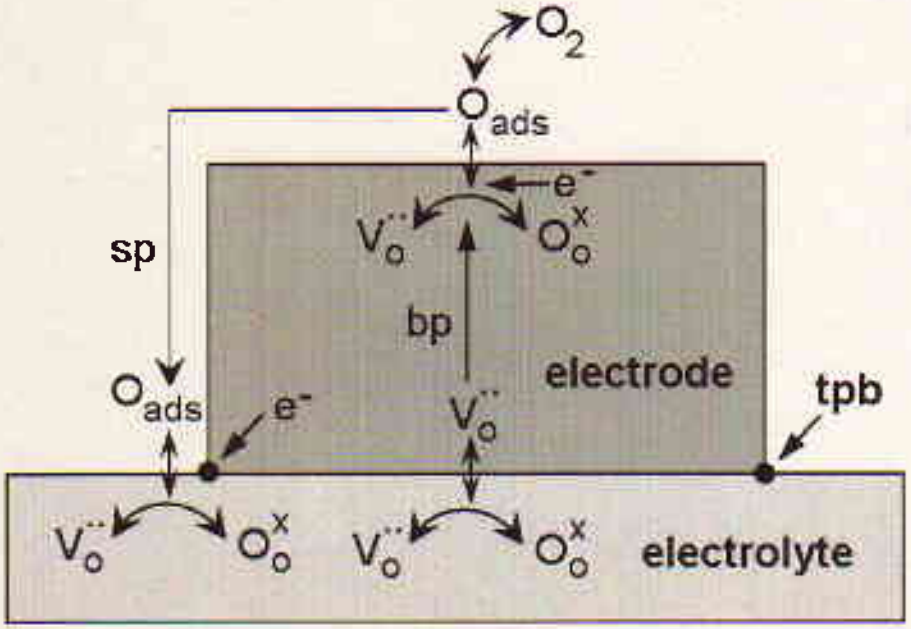

● triple phase boundary sp/bp: surface/bulk pathway

Figure 8

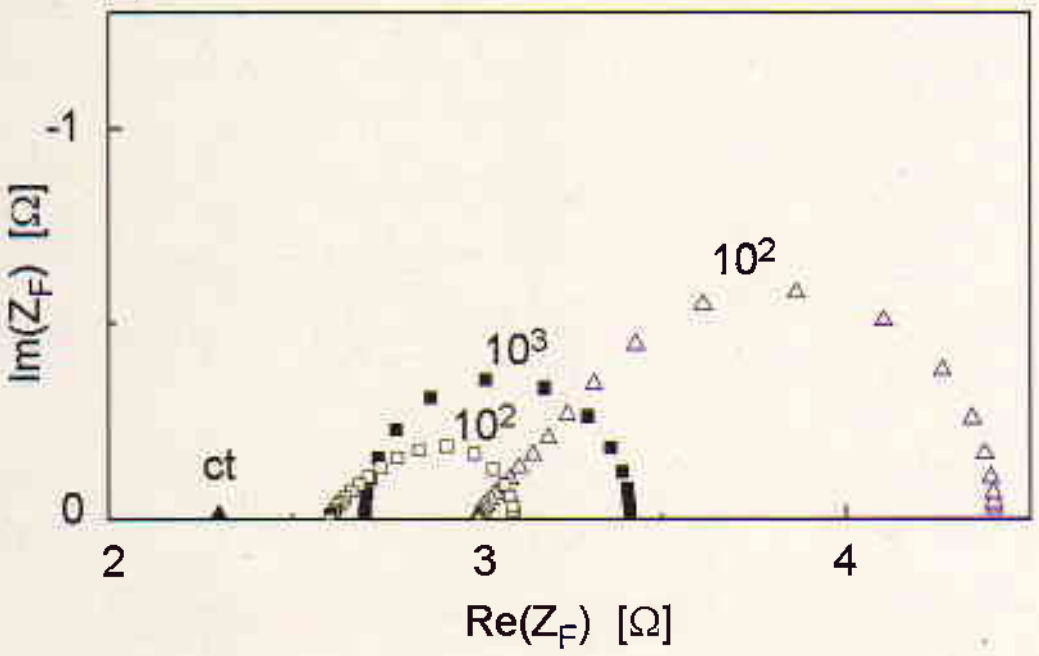

Figure 9

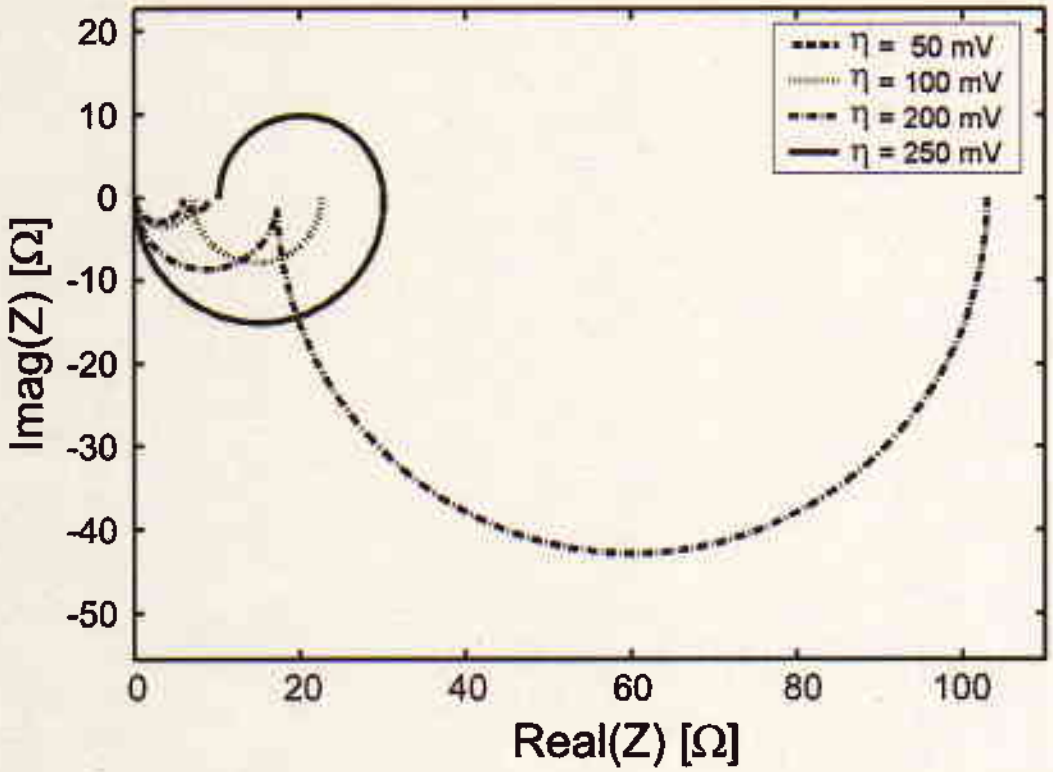
η = 50 mV
η = 100 mV
η = 200 mV
η = 250 mV
Imag(Z) [Ω]
Real(Z) [Ω]
20
10
0
-10
-20
-30
-40
-50
0
20
40
60
80
100

Figure 10

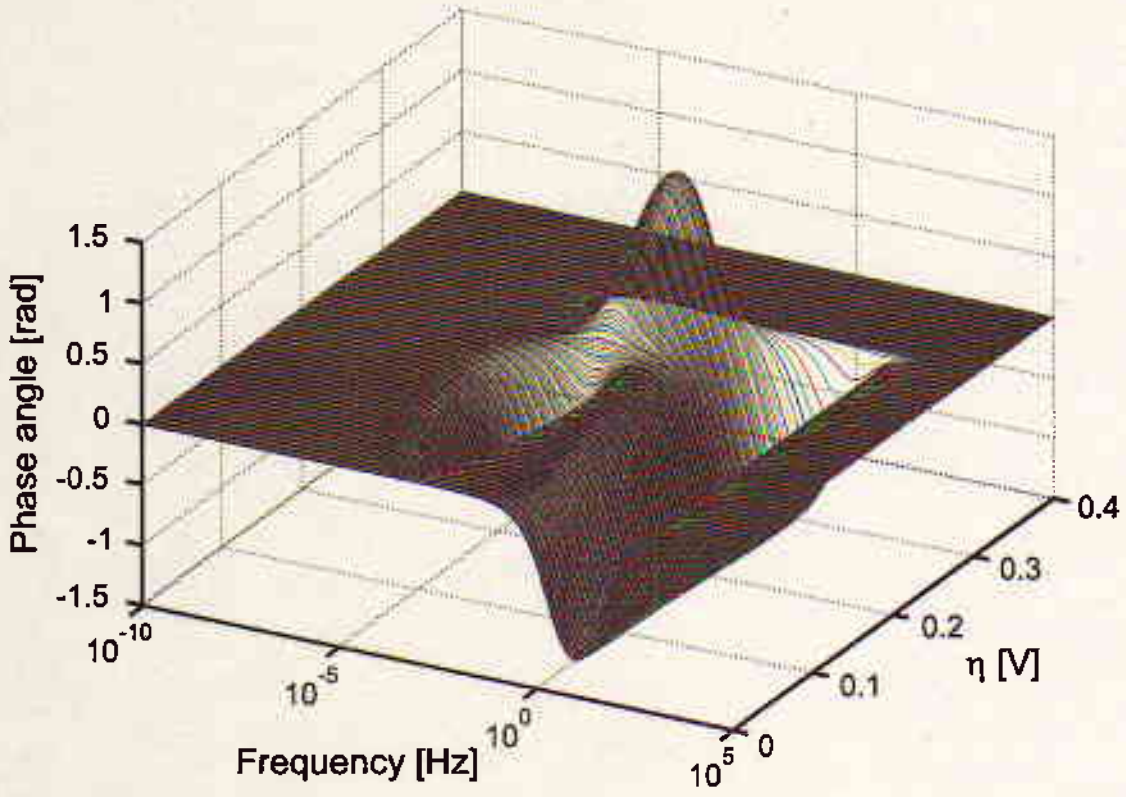
Phase angle [rad]
1.5
1
0.5
0
-0.5
-1
-1.5
10^{-10}
10^{-5}
10^{0}
10^{5}
Frequency [Hz]
0
0.1
0.2
0.3
0.4
η [V]

Figure 11

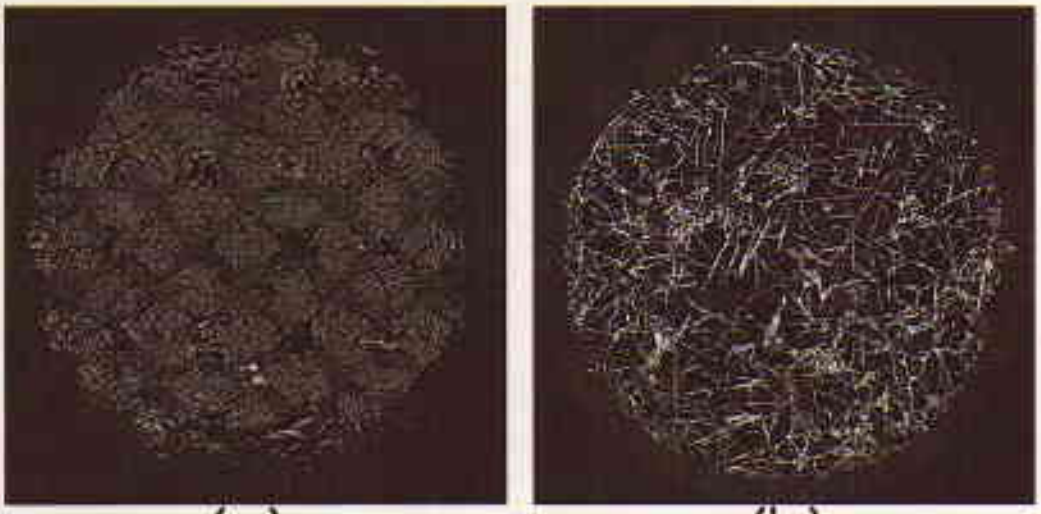

(a) (b)

Figure 12

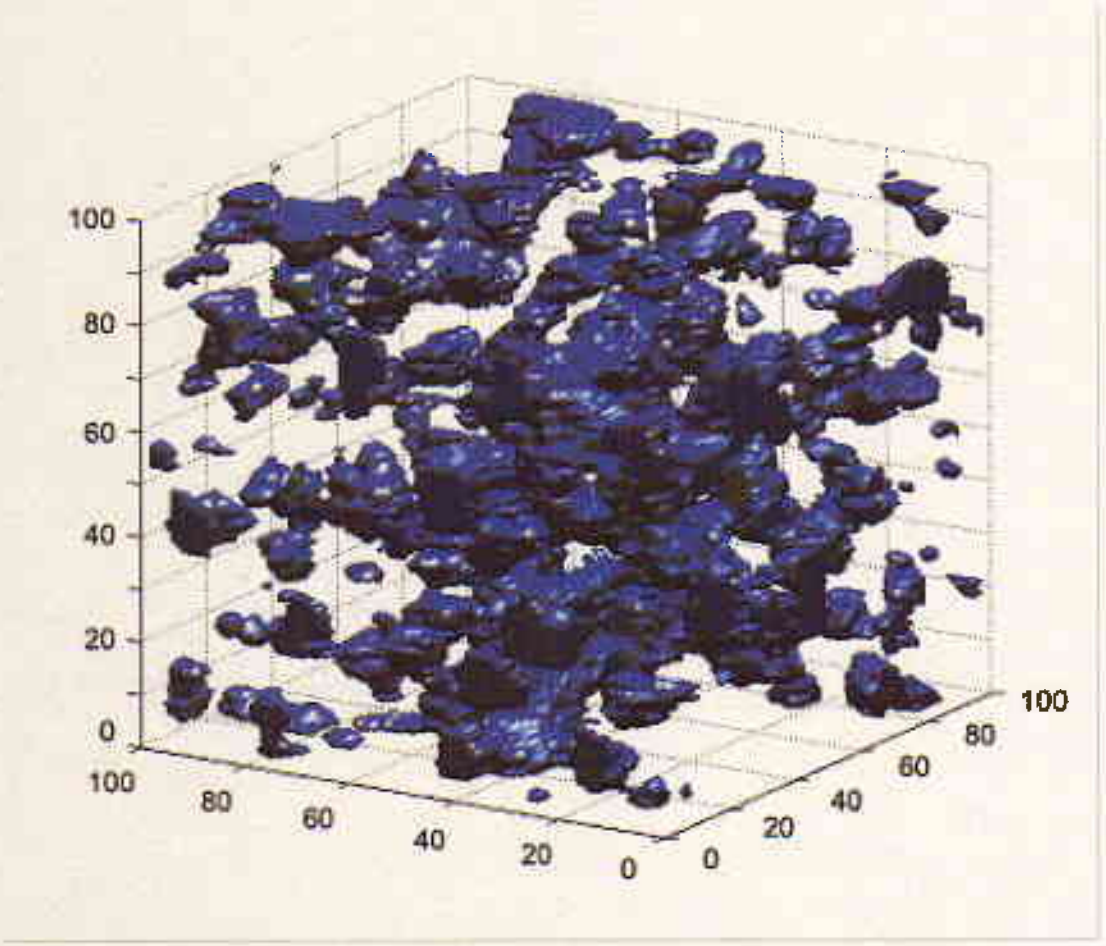

Figure 13

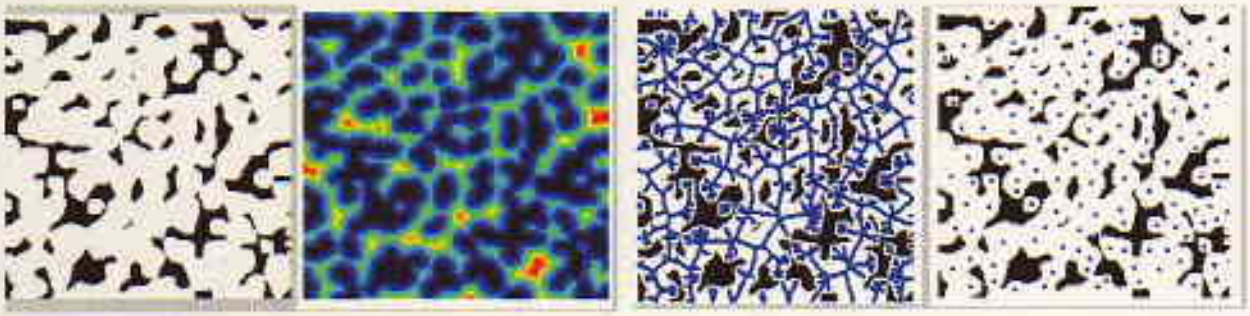

Digitized Size | Euclidian distance map | Skeleton points | Valid disc centers

Figure 14

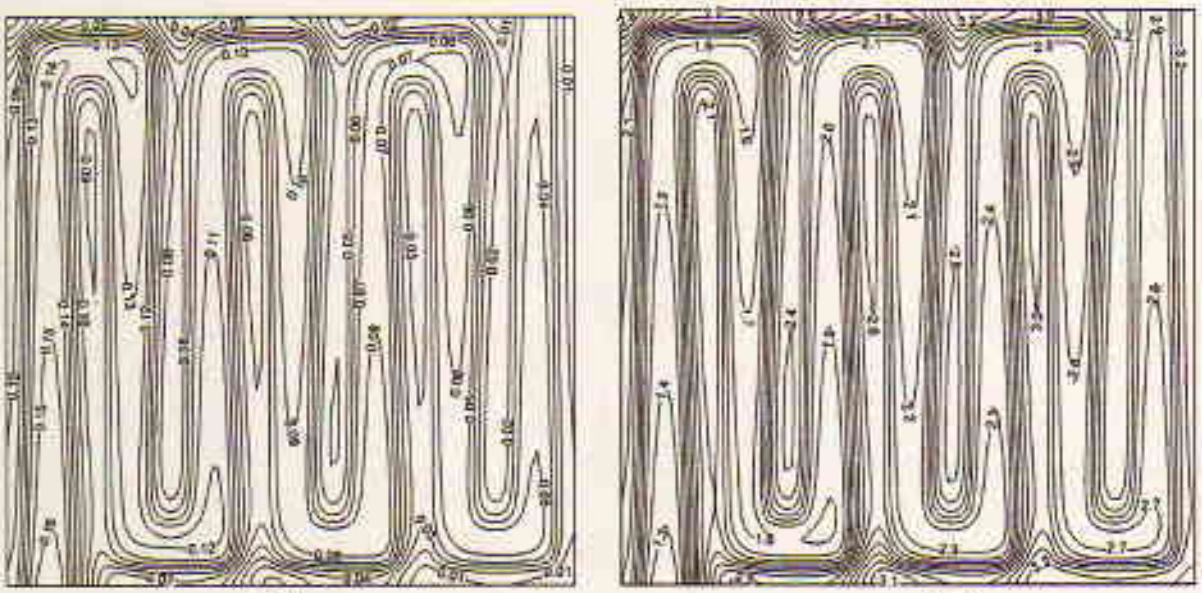

(a) (b)

Figure 15

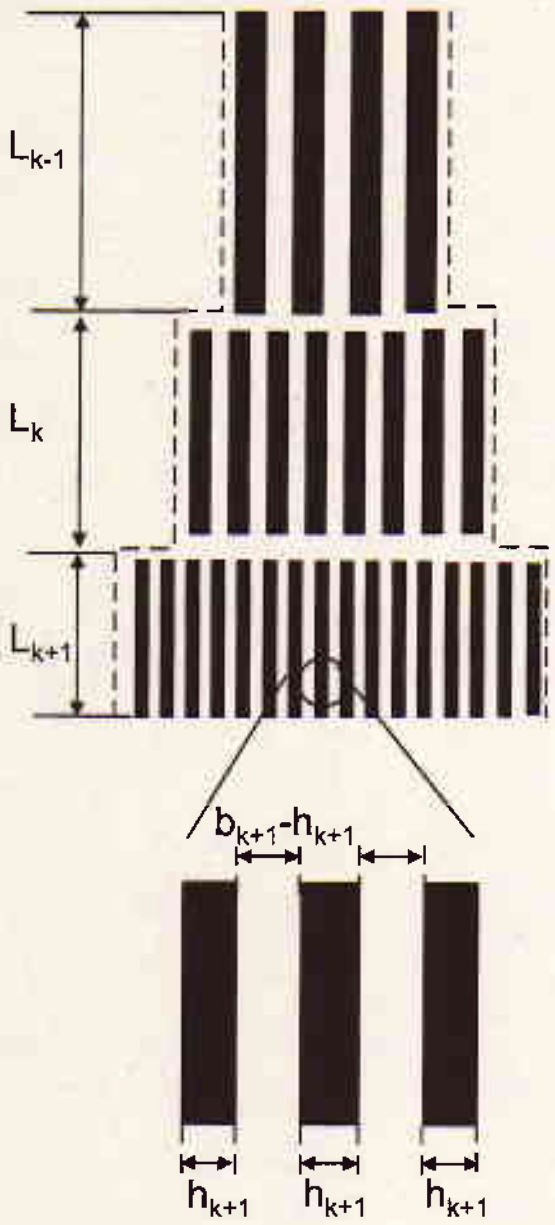

Figure 16

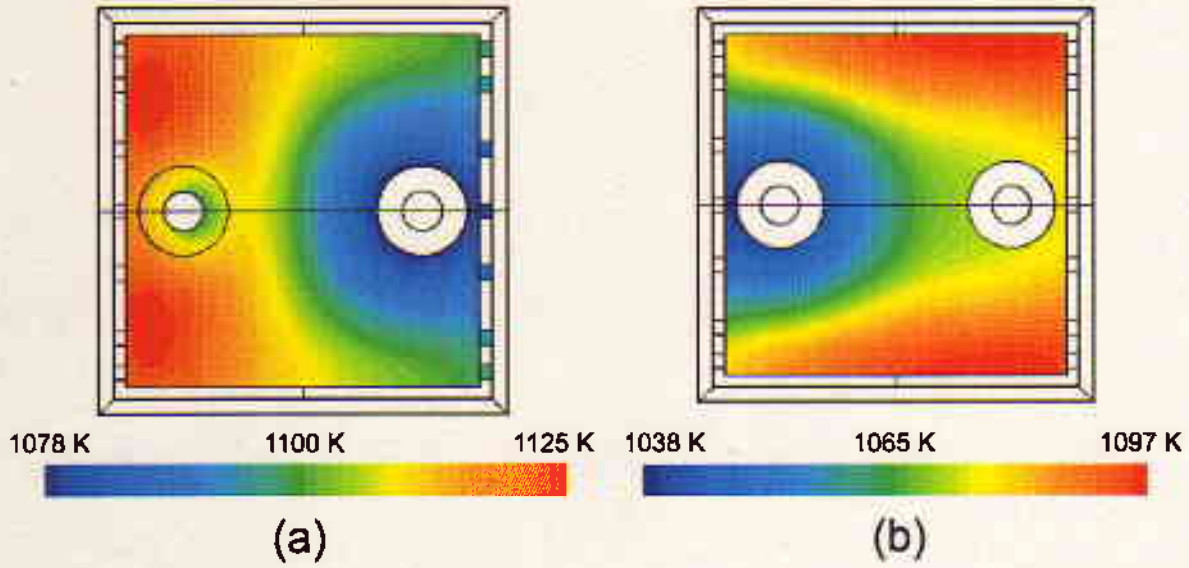

Figure 17